water

MDPI

Article

Experimental Study on Head Loss Due to Cluster of Randomly Distributed Non-Uniform Roughness Elements in Supercritical Flow

Suresh Kumar Thappeta [1,*], Peter Fiener [2] and Venu Chandra [3]

[1] Department of Geography and Environmental Development, Ben-Gurion University of the Negev, Beer Sheva 84105, Israel
[2] Institute for Geography, University of Augsburg, Postweg 118, 86159 Augsburg, Germany; peter.fiener@geo.uni-augsburg.de
[3] Department of Civil Engineering, Indian Institute of Technology, Madras 600036, India; vc@iitm.ac.in
* Correspondence: sthappeta@gmail.com; Tel.: +972-8-6472017

Abstract: Accurate estimation of head loss introduced via randomly placed roughness elements found in natural or constructed streams (e.g., fish passages) is essential in order to estimate flow variables in mountain streams, understand formation of niches for aquatic life, and model flow structure. Owing to the complexity of the involved processes and the often missing detailed data regarding the roughness elements, the head loss in such streams is mostly approximated using empirical models. In our study, we utilize flume experiments to analyze the effects of the spatial distribution of roughness elements on water surface levels and head loss and, moreover, use the produced data to test three empirical models estimating head loss. The experiments were performed in a 15 m long, 0.9 m wide flume with a slope of 5% under large Froude numbers (2.5–2.8). Flow velocities and water levels were measured with different flow rates at 58 points within a 3.96 m test section of the flume. We could show that different randomly arranged patterns of roughness elements significantly affected head loss (differences up to 33.6%), whereas water jumps occurred when flow depths were in the same size range as the roughness elements. The roughness element position and its size influenced water surface profiles. None of the three tested empirical models were able to well reproduce the differences in head loss due to the different patterns of roughness elements, with overestimated head loss from 12 to 94.7%, R^2 from 41 to 73%, *NSE* from −21.1 to 0.09, and *RRMSE* from 18.4 to 93%. This generally indicates that these empirical models are conditionally suitable to consider head loss effects of random patterns of roughness elements.

Keywords: non-uniform size boulders; random patterns; water depth; supercritical flow; head loss

check for updates

Citation: Thappeta, S.K.; Fiener, P.; Chandra, V. Experimental Study on Head Loss Due to Cluster of Randomly Distributed Non-Uniform Roughness Elements in Supercritical Flow. *Water* **2022**, *14*, 464. https://doi.org/10.3390/w14030464

Academic Editor: Mauro De Marchis

Received: 15 December 2021
Accepted: 30 January 2022
Published: 4 February 2022

Publisher's Note: MDPI stays neutral with regard to jurisdictional claims in published maps and institutional affiliations.

Copyright: © 2022 by the authors. Licensee MDPI, Basel, Switzerland. This article is an open access article distributed under the terms and conditions of the Creative Commons Attribution (CC BY) license (https://creativecommons.org/licenses/by/4.0/).

1. Introduction

The spatio-temporal dynamics of the flow depths and velocities in mountainous streams are influenced by cobbles, boulders, and step pools. The cobbles, boulders, and step pools cause head loss along the stream flow pathway [1–5], and understanding the spatio-temporal flow dynamics is essential for modelling [6]. The highly variable flow velocities and flow depths form niches for different flora and fauna, and are important to fish lifecycles [7] and biodiversity in general [8,9]. A thorough investigation is required on the ecology and morphology of watershed and streams [10,11] in order to make any changes in this region that help mankind with hydraulic and hydrologic knowledge about mountain streams [1,12,13]. The stream flow depth and its velocity are important for assessing the morphological response of streams [14], as well as to design fish passages [15–17].

The Mannings and Darcy–Weisbach models are generally used for estimating head loss in open-channel flows. However, these models cannot be used when vortices formed in the wake region of macro-roughness elements [18,19]. For supercritical flows, the Darcy–Weisbach friction factor can be estimated using empirical models developed based on the

field data when boulders are in the submerged condition [2,5,20]. In earlier studies, it was assumed that the roughness elements were submerged and the proposed models are valid for such flow conditions. However, the roughness elements present in mountainous streams are partially exposed to the atmosphere and few are in submerged conditions. The relative submergence significantly influences the head loss, which is a function of both stream flow depth and effective diameter of macro-roughness elements [2]. In a typical mountain stream, macro-roughness elements are non-uniformly sized and are randomly distributed. Recent experimental studies [14–16,18,21–23] have considered different characteristics of both flow and macro-roughness elements to estimate head loss (Table 1). Different types of empirical models were proposed to estimate the head loss caused by macro-roughness elements in mountainous streams [23–25]. Moreover, Baki et al. [15,26] and Cassan et al. [27] also developed models to find head losses in fish passages. In these studies, empirical models were developed by considering the channel slope, flow velocity, flow depth, cluster density, size, and spatial distribution of roughness elements. However, the effect of random distribution of non-uniform sized macro-roughness elements for a given cluster density was not investigated in any of the above mentioned studies. Understanding empirically the importance of randomness of roughness elements in the head loss models is still necessary. However, nowadays, the flow resistance due to the presence of roughness elements has been studied widely using 3D computational fluid dynamics (CFD) models [25,26,28].

In this paper, flume experiments are focused on three random distribution/patterns of non-uniform size roughness elements under super critical flow conditions. An investigation was undertaken to study how random patterns of roughness elements affect head loss for a given cluster density. The proposed empirical models in the literature [23,25,27] are chosen based on the applicability of current experimental conditions and tested using the flume experimental data. As our flume experiments are limited to a single constant cluster density, this study aims (1) to experimentally analyse the effect of random distributions or patterns of non-uniform size roughness elements under supercritical flow conditions on surface water levels and head loss, and (2) test available empirical models in the literature that are proposed to estimate head loss in natural or constructed streams.

Table 1. Experimental investigation on head loss due to macro roughness elements.

Flume Characteristics			Details of Macro Roughness Element's				Flow Characteristics			Authors
Length	**Width**	**Bed Slope**	**Shape**	**Diameter**	**Distribution**	**Cluster Density Range †**	**Flow Rate**	**Relative Submergence ‡**	**Froude Number**	
m	**m**	**%**	**–**	**m**	**–**	**%**	**m^3/s**	**–**	**–**	**–**
3.5, 6, and 9	0.25, 0.35, and 0.5	8, 18, 25, and 40	Hemi sphere	0.029 and 0.038	Random	0–30	–	0.5–10.5	0.8–2.8	Pagliara and Chiavaccii [23]
12	2	0.001 and 0.005	Hemi sphere	0.054 and 0.116	Random	2.9–74.9	0.0004–0.0105	0.4–2.0	<1	Jordanova [19]
8.89	0.92	1.5, 3, and 5	Sphere	0.12–0.16	Structured	–	0.0250–0.1600	0.77–1.6	0.39–0.78	Baki et al. [15]
8.89	0.92	1.5	Sphere	0.14	Structured	–	0.1400–0.1980	1.56–1.90	<1	Baki et al. [21]
7 and 10	0.25 and 1	1–9	Cylinder	0.035 and 0.115	Structured	8–16	0.0100–0.0900	0.3–2.8	0.14–1.8	Cassan et al. [16]
4	0.4	1–9	Cylinder	0.035	Structured	8–19	0.0010–0.0180	>1	0.2–1.4	Cassan and Laurens [20]
7	0.92	5	Sphere	0.036–0.498	Random	0.7–16, 44	0.05–0.45	0.2–2.4	1.2–2.8	Thappeta et al. [25] *

† Cluster density is the ratio between area occupied by the roughness elements and the encompassed cluster area; ‡ relative submergence is the ratio between flow depth measured from channel bottom and size of the roughness element. * This study is based on numerical experiments.

2. Methodology

2.1. Experimental Setup

Experiments were conducted in a horizontal rectangular flume with a length of 15 m and width of 0.9 m. An acrylic sheet was used to obtain a bed slope of 5% [2,15], which helps to create supercritical flow. This inclined false bottom surface has a length of 10 m, as shown in Figure 1. The flow that enters the flume is free from the flow disturbances because the upstream tank is located at a distance of 6.7 m from the flume entrance. Two centrifugal pumps with 25 HP capacity each were used to recirculate the flow. A test section of 3.96 m length starts at a distance of 3.38 m from the flume entrance (Figure 1). Spherical stainless-steel balls of size ranging from 0.0254 to 0.106 m were considered as roughness elements, placed randomly in three different patterns; planes 1, 2, 3, 4, and 5 in the flow direction were defined in the test section (Figure 2). The number of roughness elements (N = 6) and the cluster density (λ = 3%; Equations (1) and (2)) were kept constant for all of the experiments.

$$\lambda = \frac{N\frac{\pi}{4}{D_{eff}}^2}{l \cdot b} = 3\% \quad (1)$$

$$D_{eff} = \sqrt{\frac{D_1^2 + D_2^2 + \cdots + D_N^2}{N}} = 0.067 \text{ m} \quad (2)$$

where, D_1, D_2, D_3 … D_N are the individual diameters of the roughness elements *R1, R2, R3 … RN*, respectively, and D_{eff} is the effective diameter. Among the six roughness elements, D_1 is the largest size; D_3 and D_6 are 72% of D_1; D_5 is the medium size (48% of D_1); and D_2 and D_4 are the smallest size (24% of D_1). These sizes were selected randomly. In the three patterns, the position of the largest size (D_1 = 0.106 m) *R1* was changed along the central plane 3, in order to avoid disturbances near the boundary (Figure 2). The position of *R2*, *R3*, and *R6* in the test section was changed for the three patterns, but the position of *R4* and *R5* was unchanged. The cluster length l (1.350 m) represents the longitudinal distance between the starting point of the first boulder and the end point of the last boulder, and the cluster width b (0.575 m) represents the lateral distance between the left-most and the right-most boulders. Grid width (0.15 m) was not varied in the flow direction until 5.73 m, whereas it was changed in the transverse direction. The roughness elements were placed away from the side walls of the flume to avoid the wall effect. Three flow rates were used in this study (0.110, 0.121, and 0.131 m^3/s). Corresponding relative submergence [25] was calculated using Equation (3), resulting in 0.93, 1.00, and 1.09 (Table 2).

$$\text{Relative submergence} = (H_u / D_{eff}) \quad (3)$$

where H_u is the flow depth of the approaching flow at the upstream of the roughness elements.

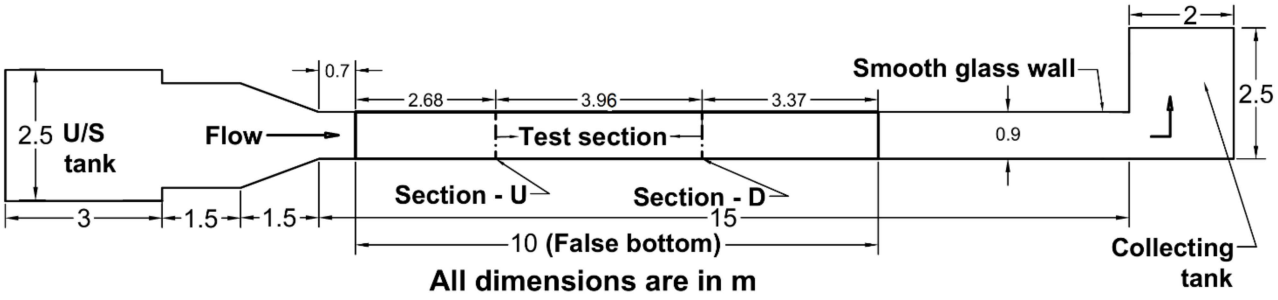

Figure 1. Experimental setup plan view.

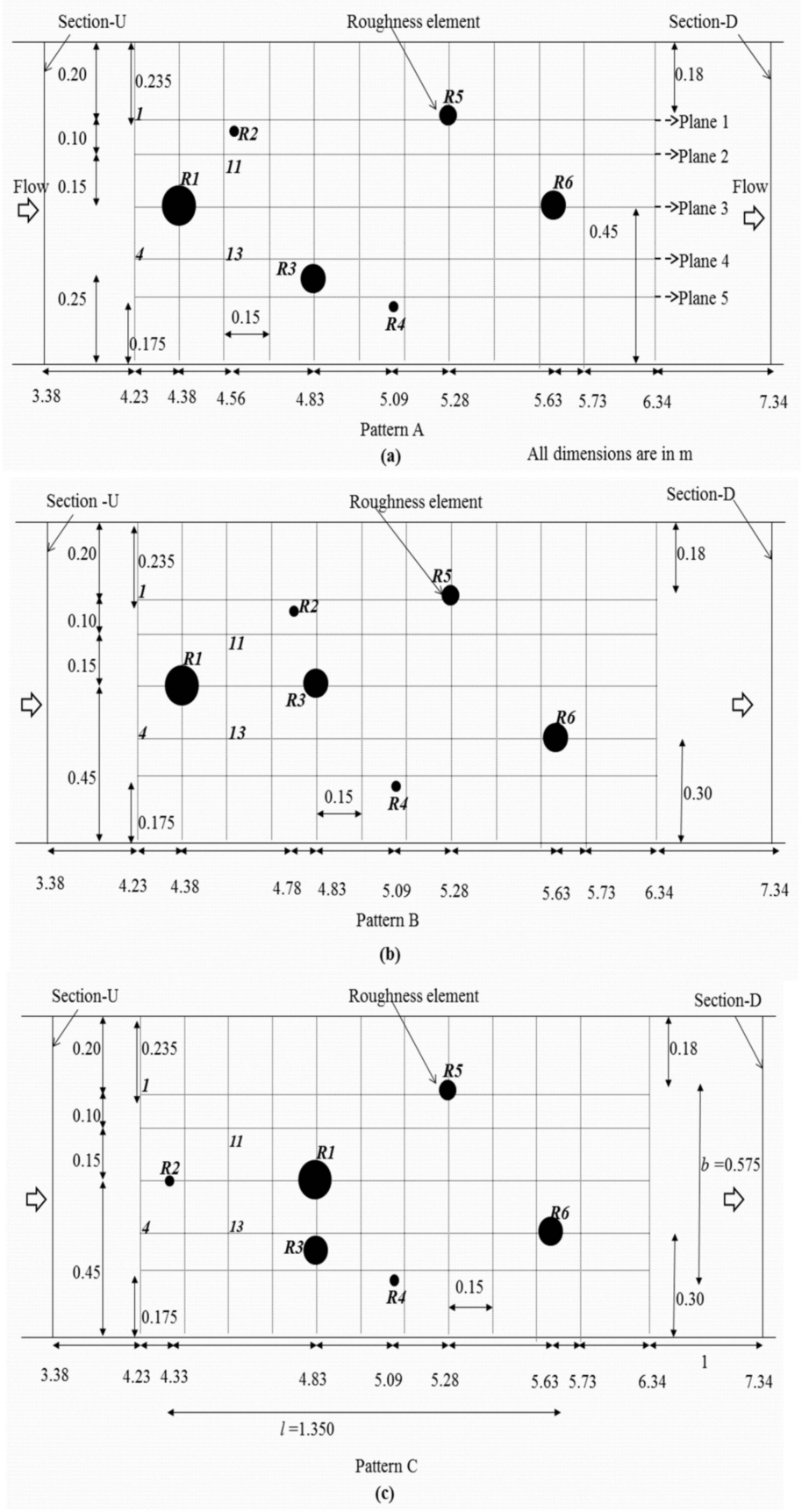

Figure 2. Different roughness element patterns: (**a**) pattern A; (**b**) pattern B; (**c**) pattern C.

Table 2. Details of various experimental parameters.

Pattern	Flow Rate (m ^{3}/s)	Average Flow Depth at "Section-U" H_u (m)	Relative Submergence H_u/D_{eff}	Froude Number at "Section-U" F_u	Cluster Density λ (%)
A, B, and C	0.110	0.0616	0.93	2.71	3
	0.121	0.0666	1.00	2.65	3
	0.131	0.0721	1.09	2.56	3

2.2. Measurements

An ultrasonic flow meter (UFM 6760, Adept Fluidyne, Pune, India) with an accuracy of ±1% was used to control the flow rate delivered by the pumps. The flow velocity and water levels were measured at 58 grid points in the test section (Figure 2) using an Acoustic Doppler Velocimeter (ADV; Model N4000-72, Nortek, Boston, USA) fitted to an automatic traverse system and a digital point gage (Model SDV-24E -vertical; Mitutoyo, Kanagawa, Japan), respectively. The grid was prepared in such a way that the ADV can measure the velocity data without any difficulty owing to the presence of roughness elements. A probe check was carried out to confirm the signal strength as per the guidelines of the instrument. The digital point gage can measure water depth up to 0.6 m with an accuracy of $\pm 0.05 \times 10^{-3}$ m. The water level at each grid point was measured three times to avoid errors and an average value was taken. The ADV data were despiked as per Goring and Nikora [29] standards before using the data for further analysis, as discussed below. The 3D point velocities along the flow depth at each grid point were measured at an interval of 0.005 m starting from the flume bed using an ADV side looking probe with a sampling frequency of 25 Hz. The temporal mean velocity was unchanged beyond a sampling period of 180 s. The velocity data recorded by the ADV have shown a correlation coefficient (COR) and signal-to-noise ratio (SNR) between 40% and 90% and 15 and 25 dB, respectively. For highly turbulent and aerated flow, the COR and SNR values were reported as up to 30% and 5 dB, respectively [30]. Initially, the measured velocity data were passed through a filtering scheme of SNR ≥15 dB and COR ≥40%, and the spikes were eliminated [29]. The total head at any section along the flow is the summation of datum head, pressure head, and velocity head. The total head at upstream (section-U) and downstream (section-D) sections is denoted as TE_u and TE_d, respectively (Figures 1 and 2). Subscripts 'u' and 'd' denote the upstream and downstream sections of the channel, respectively. The total head loss ($\Delta TE = TE_d - TE_u$) occurs owing to the presence of both roughness elements (ΔE) and bed friction (ΔE_{bed}). The head loss due to bed friction (ΔE_{bed}) was calculated using experimental data obtained without roughness elements, and ΔE_{bed} was found to be 0.058 m, 0.048 m, and 0.046 m for a flume discharge of 0.110, 0.121, and 0.131 m^3/s, respectively. The Mannings n is equal to 0.01, calculated from the flow data without roughness elements. Later, ΔE can be calculated ($\Delta E = \Delta TE - \Delta E_{bed}$). The Froude number ($F_u$) of our study varied over a small range from 2.56 to 2.71. For our flume experimental conditions, it is found that velocity profiles using an ADV side looking probe can be measured accurately for a minimum flow depth of 0.0616 m and the corresponding F_u is 2.71, whereas 2.56 is fixed based on the maximum allowed flow rate of 0.131 m^3/s.

2.3. Proposed Empirical Models

The following empirical formulae were proposed by different authors to find the increase in Darcy–Weisbach friction factor (f_i), head loss (ΔE), and flow rate (q) due to presence of roughness elements valid for supercritical flow. However, we converted them to the total head loss (ΔTE) using the well-known general Equations (13)–(15) and compared them with our observed total head loss data. The detailed comparison and corresponding error for different patterns are listed in Table 3.

Table 3. Comparison of total head loss (ΔTE) with the models reported in the literature.

	Present Experimental Study Observations				**Pagliara and Chinvacini [23] Model** $f_i = c\lambda^d$ **(**c **= 0.6;** d **= 0.7)**				**Cassan et al. [27] Model** $q=\sqrt{\frac{2gS_o(1-\lambda)}{C_D f(F_c) f\left(\frac{H_u}{D_{eff}}\right)\frac{C_r}{D_{eff}}+\beta\frac{B_f}{H_u}}}H_u$ g**=9.81 m/s^2;** S_o**=0.05;** C_r**=0.006;** C_D**=0.3;** D_{eff}**=0.067 m;** β**=0.935;** B**=0.005**			**Thappeta et al. [25] Model** $\Delta TE = \Delta E + \Delta E_{bed}$ $\Delta E = I[N][\Delta E_{sr}]$ N**=6**		
Pattern	Q	V_u	ΔE_{bed}	ΔTE	f_i	ΔE	ΔTE	**Error**	q	ΔTE	**Error**	ΔE	ΔTE	**Error**
	(m^3/s)	**(m/s)**	**(m)**	**(m)**	**-**	**(m)**	**(m)**	**(%)**	**(m^2/s)**	**(m)**	**(%)**	**(m)**	**(m)**	**(%)**
A	0.110	1.98	0.058	0.131	0.050	0.187	0.243	−85	0.187	0.167	−22	0.092	0.150	−12
	0.121	2.02	0.048	0.110	0.050	0.170	0.217	−97	0.232	0.153	−28	0.082	0.130	−15
	0.131	2.02	0.046	0.092	0.050	0.170	0.212	−130	0.225	0.144	−36	0.074	0.120	−23
B	0.110	1.98	0.058	0.124	0.050	0.187	0.243	−96	0.187	0.167	−26	0.092	0.150	−17
	0.121	2.02	0.048	0.127	0.050	0.170	0.217	−71	0.232	0.153	−17	0.082	0.130	−2
	0.131	2.02	0.046	0.095	0.050	0.170	0.212	−123	0.235	0.144	−34	0.074	0.120	−20
C	0.110	1.98	0.058	0.154	0.050	0.187	0.243	−58	0.187	0.167	−7.9	0.092	0.150	+2
	0.121	2.02	0.048	0.147	0.050	0.170	0.217	−48	0.232	0.153	−4	0.082	0.130	+11
	0.131	2.02	0.046	0.087	0.050	0.170	0.212	−144	0.225	0.144	−39	0.074	0.120	−27

Pagliara and Chiavaccini [23] model:

$$f_i = c\lambda^d \tag{4}$$

Thappeta et al. [25] models:

$$\Delta E = I[N][\Delta E_{sr}] \tag{5}$$

$$I = 2.0(\lambda)^{-0.37} F_u{}^{0.22}\left(\frac{H_u}{D_{eff}}\right)^{-0.57}\left(\frac{H_u}{LD}\right)^{1.00} \tag{6}$$

$$\Delta E_{sr} = LD\left[0.062 \times F_u{}^{1.42}\left(\frac{H_u}{D_{eff}}\right)^{-1.61}\left(\frac{H_u}{LD}\right)^{0.88}\right] \tag{7}$$

Cassan et al. [27] models:

$$q = \sqrt{\frac{2gS_o(1-\lambda)}{C_D f(F_c) f\left(\frac{H_u}{D_{eff}}\right)\frac{C_r}{D_{eff}}+\beta\frac{B_f}{H_u}}}H_u \tag{8}$$

$$B_f = \frac{2}{\left(5.1log\left(\frac{H_u}{k_s}\right)+6\right)^2} \tag{9}$$

$$f(F_c) = min\left(\frac{1}{1-\frac{F_c^2}{4}}, \frac{1}{F_c^{0.67}}\right)^2 \tag{10}$$

$$F_c = \frac{F_u}{1-\sqrt{\frac{C_r\, l}{b}}} \tag{11}$$

$$f\left(\frac{H_u}{D_{eff}}\right) = 1+\frac{0.4}{\left(\frac{H_u}{D_{eff}}\right)^2} \tag{12}$$

General models:

$$\Delta E = \frac{f_i L V_u^2}{8gR} \tag{13}$$

$$\Delta TE = \Delta E + \Delta E_{bed} \tag{14}$$

$$\Delta TE = \frac{q^2 n^2 L}{H_u^{10/3}} \tag{15}$$

where f_i = increase in Darcy–Weisbach friction factor due to roughness elements; c = 0.6; d = 0.7; I = interaction factor; ΔE_{sr} = head loss due to a single roughness element; F_u = Froude number; F_c= correction factor for F_u; LD = longitudinal distance from section-U to the nearest boulder (for the present study, LD = 0.947 m); g = 9.81 m/s^2; S_o = bed slope; $C_r = \frac{D_{eff}{}^2}{lb}$ = roughness elements concentration assuming l, b are equal to the cluster center-center distance of in longitudinal and lateral direction, respectively; C_D = drag coefficient (=0.3 for spherical shape roughness element [31]); $\beta = 1 - \sqrt{\frac{C_r b}{l}} - \frac{(\lambda)}{2}$; $\frac{H_u}{D_{eff}}$ = relative submergence; B_f = bed friction factor; $f(F_c)$ = correction function to consider the influence of Froude number on flow resistance; $f\left(\frac{H_u}{D_{eff}}\right)$ = correction function to consider the interaction between flow and channel bed; q = flow rate per unit width; L = length of test section; n = Mannings roughness value; $k_s = \left(6.7n\sqrt{g}\right)^6$ = equivalent sand grain size roughness value; V_u = averaged velocity; and R = hydraulic radius. Subscripts 'u' and 'd' denote upstream and downstream sections of the channel, respectively, as mentioned earlier. Pagliara and Chiavaccini [23] model was developed based on purely empirical data. Cassan et al. [27] model was a semi-analytical one based on momentum balance and experimental data. Accurate selection of functional relation for B_f is an important aspect while estimating head loss. Equation (9), used in our study, can accurately estimate bed friction for hydrodynamically rough bed with roughness elements. However, Blasius formula can be used for the hydrodynamically smooth bed where flow is smooth [16]. The study of Thappeta et al. [25] is based on complete numerical experiments using the 3D CFD ANSYS-CFX model. Thus, we considered three forms of head loss models to test the random pattern effect on head loss.

3. Results

3.1. Water Surface and Velocity Profiles

Figure 3 shows experimental images for a flow rate of 0.110 and 0.131 m^3/s. For pattern A (Figure 3a,b), it can be observed that the roughness element *R3* was in submerged condition when the discharge was increased from 0.110 to 0.131 m^3/s. However, at the same flow rate for pattern C, a water jump has not formed at *R3* owing to a change in the position of *R1* (Figure 3e). Meanwhile, in pattern B, the water jump formed over roughness elements (*R3* and *R6*), which may be because of the upstream protruding boulder *R1* (Figure 3c,d). For pattern C, the water jump does not form over *R3*, although the discharge increased, but no protruding boulder was present upstream of the same plane (Figure 3f). It can be inferred that the position of the roughness elements (especially *R1*) and discharge (or Froude number) together influenced the formation of the water jump, and thus the flow structure, although the cluster density was unchanged. The water jumped over the boulder in the form of a jet and splashed onto the downstream water pool at some distance from the boulder when flow depth (y) was less than D. Such water jumps occurred noticeably along plane 3 for all the three patterns.

Figure 4 shows the water surface profiles in four planes for the three patterns of roughness elements for a constant discharge (Q = 0.110 m^3/s) and cluster density. The profiles along plane 3 were shown separately in Figure 5 owing to water jump formation. A maximum water surface level of 0.064, 0.068, and 0.066 m along plane 1 was observed owing to the presence of *R5* at 5.28 m longitudinal distance for patterns A, B, and C, respectively (Figure 4a). However, the water surface levels dropped before and after the roughness element. For pattern A and B, the water surface profiles along plane 1 and 2 did not vary significantly. This is because of the unchanged position of largest roughness element *R1* (Figure 4a,b). Meanwhile, a significant difference was observed for pattern A and B along plane 4 and 5 due to the jump formation over *R3* at 4.83 m in pattern A, and no jump in pattern B (Figure 4c,d). Although the roughness elements were not present in plane 2, the variation in the water surface profiles can be noticed in pattern C because of adjacent roughness elements *R1, R2*, *R3*, *R5,* and *R6*. However, it was observed that the change in the magnitude of water surface level depends on both position and

size of the roughness element (Figure 4). For pattern A along plane 4, the water level suddenly dropped to 0.047 m at a distance of 5.13 m owing to the jump formation over *R3*, which leads to the discontinuity in the water depth. Meanwhile, for other patterns at 4.98 m onward, the water surface profiles are unchanged owing to no such water depth discontinuity because of the change in the position of *R1* and *R3* (Figure 4c). A similar observation was noticed along plane 5, whereas water level suddenly dropped for pattern A (Figure 4d). However, all water surface profiles were not identical for a given plane, discharge, and cluster density when the pattern is different (Figure 4). Therefore, as hypothesized, the three patterns/position of roughness element influenced the observed water surface levels spatially.

Figure 3. Experimental images: (**a**) pattern A, Q = 0.110 m^3/s; (**b**) pattern A, Q = 0.131m^3/s; (**c**) pattern B, Q = 0.110 m^3/s; (**d**) pattern B, Q = 0.131 m^3/s; (**e**) pattern C, Q = 0.110 m^3/s; (**f**) pattern C, Q = 0.131 m^3/s.

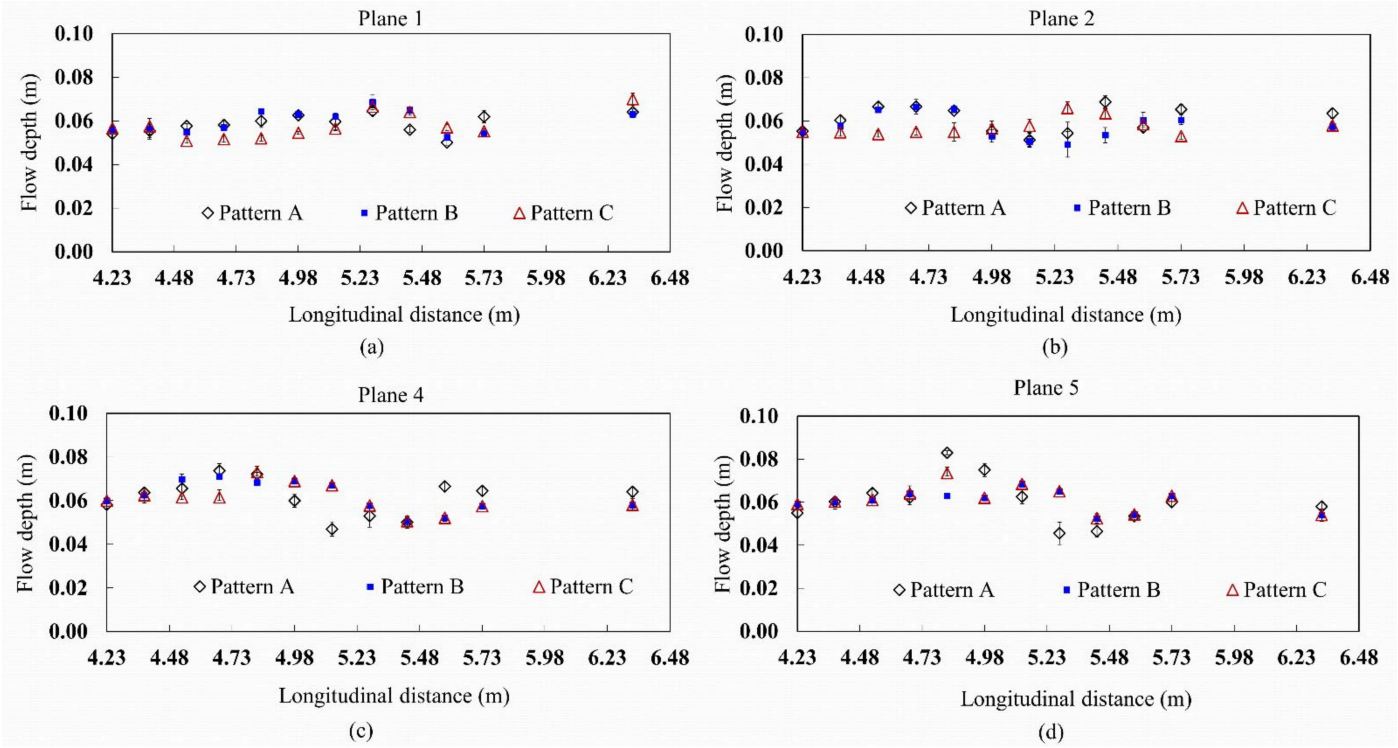

Figure 4. Observed water surface profiles for pattern A, B, and C when Q = 0.110 m^3/s: (**a**) plane 1; (**b**) plane 2; (**c**) plane 4; and (**d**) plane 5. The uncertainty associated with the water level measurements is shown as error bars.

Water jump formation was also evident in the water surface profiles along plane 3 for Q = 0.110 m^3/s (Figure 5), regardless of roughness element pattern. Jets were formed over roughness elements *R1*, *R3*, and *R6* in all three patterns (Figure 5). Measurements were taken to delineate multiple free surfaces, i.e., the lower and the upper nappes of the jets, and the free surface of the pool. The jet thickness was found to vary from 3 to 5 mm. An air pocket got formed between this water jet originating from the boulder to the downstream water pool. In pattern A, the water jet created at 4.38 m by *R1* jumped to a height of 0.18 m, and then splashed into the downstream side pool at 0.45 m from the boulder (Figure 5a). In pattern B, the water jet created at 4.38 m by *R1* splashed onto the downstream side the roughness element *R3*, and the depth of the downstream water pool between these two elements was shallow (Figure 5b). Similarly for pattern C, jump was observed at *R1*. The three patterns (especially different positions of *R1* and *R3*) caused jump formation for constant Q and cluster density.

Four representative grid points in the upstream and wake regions of the roughness elements were chosen to show velocity profiles. Two grid points (1st and 4th) were located upstream of *R1*; the other two (11th and 13th) were located downstream of *R1* (Figure 2a). The observed vertical velocity profiles for pattern A at Q = 0.110 m^3/s are shown in Supplementary Figure S1 for the grid points. No significant variation in the velocity magnitude near to bed was found at all the four grid points, which might result from the supercritical flow conditions. A similar observation is given by Cassan et al. [27].

Observations from our flume experiments indicate that the roughness elements interact with the water surface profile, giving rise to highly nonlinear spatial water surface variations when the roughness elements are just beneath the emergent conditions in supercritical flows. This interaction effect depends on the spatial locations of the non-uniformly sized elements within the cluster density for a given discharge.

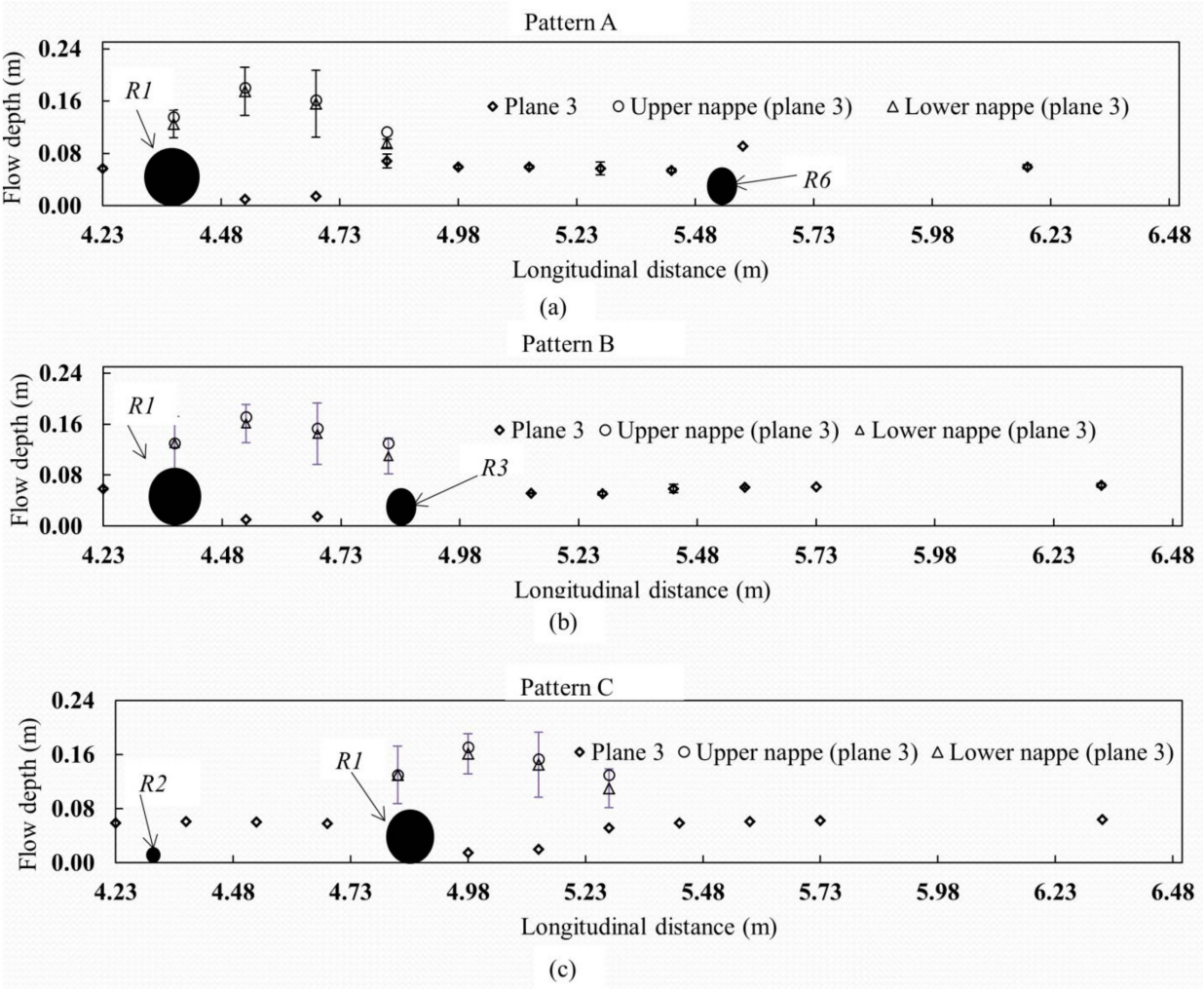

Figure 5. Water surface profiles along plane 3 for Q = 0.110 m^3/s; (**a**) pattern A; (**b**) pattern B; (**c**) pattern C. The uncertainty associated with the water level measurements is shown as error bars.

3.2. Head Loss

The total head loss induced by the bed roughness and the turbulent flow around clustered roughness elements was measured in our experiments for all three roughness patterns (Table 3). In general, our results are in line with the finding of earlier studies [15,23,32], indicating that head loss decreases with an increasing flow rate/relative submergence. Partly, the experimental results of earlier studies relating to head loss due to macro roughness elements in steep open channels were used to derive empirical models (see Equations (4)–(12)) to estimate head loss under different conditions [23,25,27]. However, as none of these models were considered a parameter for randomness, we tested these models against our experimental data. As shown in Figure 6, the empirical models were only partly able to substantially estimate the observed head loss. The model of Pagliara and Chiavaccini [23] (Equations (4), (13) and (14)) generally leads to an overestimation of the measured ΔTE (mean overestimation 94.7 $\pm$ 32.9% (Table 3)). There is some explanatory power of the model, giving an R^2 of 42%, which describes the degree of collinearity between observed and estimated ΔTE, and larger values of R^2 can be obtained even that model estimations differ considerably in magnitude [33]; overall, however, the model performance is weak given an *NSE* of $-$21.1 and an RRMSE of 93%. The model of Cassan et al. [27] (Equations (8)–(12) and (15)) also leads to an overestimation of the measured ΔTE (mean overestimation 24 $\pm$ 12% (Table 3)). There is some explanatory power of the model giving an R^2 of 58%; overall, however, the model performance is also weak with an *NSE* of $-$2.6 and an RRMSE of 33.5%. The empirical model of Thappeta et al. [25] (Equations (5)–(7) and (14))

leads to an overestimation of the measured ΔTE (mean overestimation 12 ± 12% (Table 3)). There is some explanatory power of the model giving an R^2 of 73%; overall, however, the model performance is better than the other two models giving an *NSE* of 0.09 and an RRMSE of 18.4%.

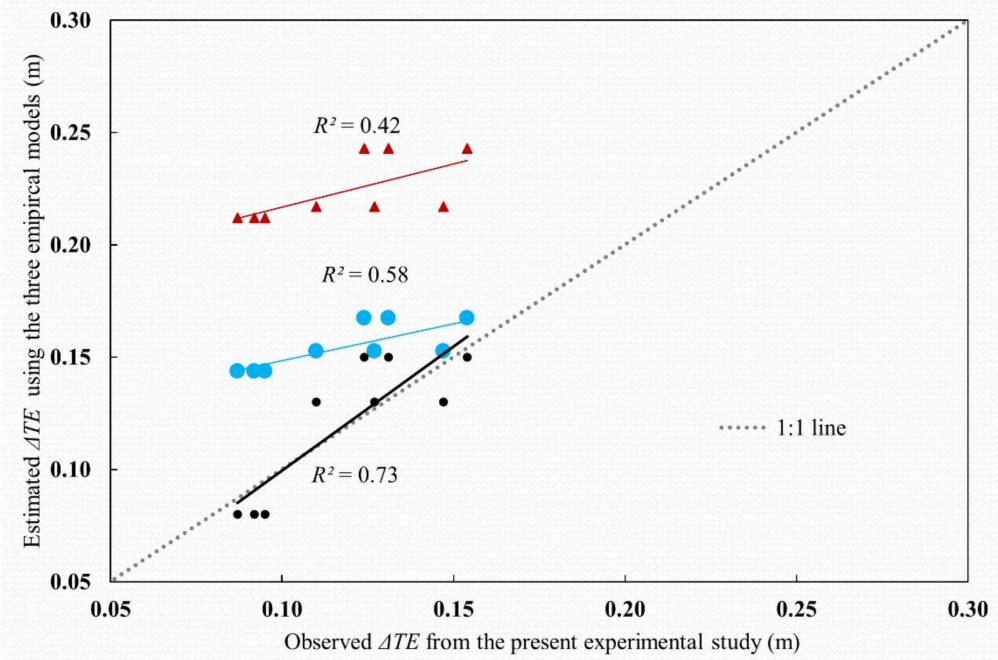

Figure 6. Comparison of observed and estimated total head loss.

4. Discussion

The results presented in the above section are discussed in the overall context of the possible reasons for overestimation of head loss by the three empirical models for our experimental work. The models do not explicitly account for patterns in random roughness elements, hence the models of Pagliaria and Chincacinin [23], Cassan et al. [27], and Thappeta et al. [25] do not show any changes in head loss with different patterns. A different general performance in estimating the head loss under supercritical flow can be recognized (Figure 6 and Table 3). This might be for several reasons. In the Pagliaria and Chincacinin [23] model: (i) f_i is a function of cluster density alone and the model does not address the effects of the approaching flow (Froude number and relative submergence); (ii) it assumes constant empirical coefficients for any random pattern of roughness elements; and (iii) hemispherical roughness elements were used in the study. In the Cassan et al. [27] model: (iv) the semi-analytical model is originally developed for the staggered pattern with uniform size roughness elements, where the present study focused on non-uniform size random patterns; and (v) both studies considered sub and superficial flows for the model development, F_u: 0.14–1.8 [27] and F_u: 0.8–2.8 [23]. (vi) λ, F_u of Cassan et al. [27] study do not fall under the range of current experimental study. However, all remaining parameters are well within the range, as are those for the Pagliara and Chiavaccini [23] and Thappeta et al. [25] study (Tables 1 and 2).

As mentioned earlier, the Thappeta et al. [25] model predicted the head loss better than the other two models, although the parameters in this model do not explicitly account for the randomness. A potential reason might be that the Thappeta et al. [25] model was developed for the Froude number (F_u) ranging from 1.20 to 2.80, considered purely supercritical flow, which is similar to this flume study. Nevertheless, the Thappeta et al. [25] model also overestimated by 12 ± 12%, which potentially results from a missing representation of different patterns of roughness elements.

From Table 3, it is observed that, for all three patterns at Q = 0.110 m^3/s, the observed ΔTE varied from 0.124 m to 0.154 m (19.5% difference). At Q = 0.121 m^3/s and

Q = 0.131 m^3/s, the observed ΔTE ranged from 0.110 to 0.147 m (33.6% difference) and from 0.087 to 0.095 m (9.2% difference), respectively. Thus, it is evident empirically that the tested three patterns affected ΔTE significantly for the given flow rate.

Overall, it is evident from our model testing that all proposed empirical models are not able to adequately represent the effects of randomly positioned roughness elements on head loss.

5. Conclusions

The objectives of the present study were to (i) understand changes in water surface levels and head losses due to the random patterns of non-uniform size roughness elements and (ii) test three different empirical head loss models. Therefore, we first conducted flume experiments under super critical flow with large Froude numbers (2.5–2.8) and measured the change in head loss in the case of different non-uniformly sized macro-roughness elements arranged in the test section. From these experiments and the model testing, we can draw the following conclusions.

Overall, significant changes in head loss (up to 33.6%) were observed in the case of all three random roughness element patterns. For the different patterns, water surface profiles were not identical for a given plane, discharge, and cluster density. The local water depth suddenly rose at the upstream and dropped at the downstream sides of the roughness element if the flow depth exceeded the size of the roughness element, whereas the formation of a water jump was noticed if the flow depth was slightly less than the size of the roughness element. In general, head loss decreased with an increase in the flow rate (or relative submergence).

The tested empirical models incurred large errors: 12–94.7%, considering the effect of the random patterns of roughness elements for a given cluster density and flow conditions.

The experimental data available from this study, especially water jump profiles at boulders, are rare for large Froude numbers, and are thus a valuable basis for further tests of empirical or three-dimensional mathematical models.

Supplementary Materials: The following supporting information can be downloaded at https://www.mdpi.com/article/10.3390/w14030464/s1. Figure S1: Observed flow velocity profiles for pattern A for Q = 0.110 m^3/s.

Author Contributions: S.K.T. was responsible for conceptualization, methodology, formal analysis, data curation, visualization, and writing the original draft. P.F. was responsible for conceptualization, methodology, and reviewing and editing the original draft. V.C. was responsible for conceptualization, methodology, resources, and reviewing and editing the original draft. All authors have read and agreed to the published version of the manuscript.

Funding: This work was funded by the Department of Science and Technology, India under grant No. DST/CCP/PR-21/2012 (C), and by the German Academic Exchange Service (DAAD) on behalf of the German Federal Ministry of Education and Research (BMBF) for the visit of Peter Fiener to Indo-German Center for Sustainability at IIT Madras.

Institutional Review Board Statement: Not applicable.

Informed Consent Statement: Not applicable.

Data Availability Statement: The data presented in this study are available in article.

Acknowledgments: We acknowledge financial support from the Indo-German Centre for Sustainability (IGCS) funded by the Department of Science and Technology, India, through the Indian Institute of Technology Madras and German Academic Exchange Service (DAAD) on behalf of the German Federal Ministry of Education and Research (BMBF).

Conflicts of Interest: The authors declare no conflict of interest.

References

1. Agostino, V.D.; Michelini, T. On kinematics and flow velocity prediction in step-pool channels. *Water Resour. Res.* **2015**, *51*, 4650–4667. [CrossRef]
2. Bathurst, J.C. Flow resistance estimation in mountain rivers. *J. Hydraul. Eng.* **1985**, *111*, 625–643. [CrossRef]
3. Comiti, F.; Mao, L.; Wilcox, A.; Wohl, E.E.; Lenzi, M.A. Field-derived relationships for flow velocity and resistance in high-gradient streams. *J. Hydrol.* **2007**, *40*, 48–62. [CrossRef]
4. Ferguson, R. Flow resistance equations for gravel- and boulder-bed streams. *Water Resour. Res.* **2007**, *43*, 1–12. [CrossRef]
5. Hey, R.D. Flow resistance in gravel-bed Rivers. *J. Hydraul. Div.* **1979**, *105*, 365–379. [CrossRef]
6. Yochum, S.E.; Bledsoe, P.B.; David, G.C.L.; Wohl, E. Velocity prediction in high gradient channels. *J. Hydrol.* **2012**, *424*, 84–98. [CrossRef]
7. Cullen, J.J. Hypotheses to explain high-nutrient conditions in the open sea. *Limnol. Oceanogr.* **1991**, *36*, 1578–1599. [CrossRef]
8. Maloney, K.O.; Munguia, P.; Mitchell, R.M. Anthropogenic disturbance and landscape patterns affect diversity patterns of aquatic benthic macroinvertebrates. *J. N. Am. Benthol. Soc.* **2011**, *30*, 284–295. [CrossRef]
9. Poff, N.L.; Zimmerman, J.K.H. Ecological responses to altered flow regimes: A literature review to inform the science and management of environmental flows. *Env. Flows Sci. Manag.* **2009**, *55*, 194–205. [CrossRef]
10. Crowder, D.W.; Diplas, P. Applying spatial hydraulic principles to quantify stream habitat. *River Res. Appl.* **2006**, *22*, 79–89. [CrossRef]
11. Hayes, J.W.; Jowett, I.G. Microhabitat models of large drift-feeding brown trout in three New Zealand rivers. *N. Am. J. Fish. Manag.* **1994**, *14*, 710–725. [CrossRef]
12. Modrick, T.M.; Georgakakos, K.P. Regional bankfull geometry relationships for southern California mountain streams and hydrologic applications. *Geomorphology* **2014**, *221*, 242–260. [CrossRef]
13. Thorne, C.R.; Zevenbergen, L.W. Estimating mean velocity in mountain rivers. *J. Hydraul. Eng.* **1985**, *111*, 612–624.
14. Chin, A. The geomorphic significance of step-pools in mountain streams. *Geomorphology* **2003**, *55*, 125–137. [CrossRef]
15. Baki, A.B.M.; Zhu, D.Z.; Rajaratnam, N. Mean flow characteristics in a rock-ramp type fish pass. *J. Hydraul. Eng.* **2014**, *140*, 156–168. [CrossRef]
16. Cassan, L.; Tien, T.; Courret, D.; Laurens, P.; Dartus, D. Hydraulic resistance of emergent macroroughness at large Froude numbers: Design of nature-like fishpasses. *J. Hydraul. Eng.* **2014**, *140*, 4014043. [CrossRef]
17. Pagliara, S.; Dazzini, D. Hydraulics of block ramp for riverrestoration. In *New Trends in Water and Environmental Engineering for Safety and Life: Eco-Compatible Solution for Aquatic Environments*; Capri, CSDU: Milano, Italy, 2002.
18. Ferguson, R. Time to abandon the Manning equation. *Earth Surf. Processes Landf.* **2010**, *35*, 1873–1876. [CrossRef]
19. Jordanova, A.A. Low Flow Hydraulics in Rivers for Environmental Applications in South Africa. Ph.D. Thesis, University of Witwatersrand, Johannesburg, South Africa, 2008.
20. Romero, M.; Revollo, N.; Molina, J. Flow resistance in steep mountain rivers in Bolivia. *J. Hydrodyn.* **2010**, *22*, 702–707. [CrossRef]
21. Baki, A.B.M.; Zhang, W.; Zhu, D.Z.; Rajaratnam, N. Flow structures in the vicinity of a submerged boulder within a boulder array. *J. Hydraul. Eng.* **2017**, *143*, 04016104. [CrossRef]
22. Cassan, L.; Laurens, P. Design of emergent and submerged rock-ramp fish passes. *Knowl. Manag. Aquat. Ecosyst.* **2016**, *417*, 45. [CrossRef]
23. Pagliara, S.; Chiavaccini, P. Flow Resistance of Rock Chutes with Protruding Boulders. *J. Hydraul. Eng.* **2006**, *6*, 545–552. [CrossRef]
24. Abdulla, A.A. Three-Dimensional Flow Model for Different Cross-Section High-Velocity Channels. Ph.D. Thesis, University of Plymouth, Plymouth, UK, 2013.
25. Thappeta, S.K.; Bhallamudi, S.M.; Fiener, P.; Narasimhan, B. Resistance in steep open channels due to randomly distributed macro roughness elements at large Froude numbers. *J. Hydrol. Eng.* **2017**, *22*, 04017052. [CrossRef]
26. Baki, A.B.M.; Zhu, D.Z.; Rajaratnam, N. Flow Simulation in a rock-ramp fish pass. *J. Hydraul. Eng.* **2016**, *142*, 4016031. [CrossRef]
27. Cassan, L.; Roux, J.; Garambois, P.A. A semi-analytical model for the hydraulic resistance due to macro-roughness of varying shapes and densities. *Water* **2017**, *9*, 637. [CrossRef]
28. Thappeta, S.K.; Bhallamudi, S.M.; Fiener, P.; Chandra, V.; Abul, B.M.B. Energy Loss in Steep Open Channels with Step-Pools. *Water* **2021**, *13*, 72. [CrossRef]
29. Goring, D.G.; Nikora, V.I. Despiking Acoustic Doppler velocimeter data. *J. Hydraul. Eng.* **2002**, *128*, 0733–9429. [CrossRef]
30. SonTek. *ADV Technical Documentation*; SonTek: San Diego, CA, USA, 1997.
31. Canovaro, F.; Paris, E.; Solari, L. Effects of macro-scale bed roughness geometry on flow resistance. *Water Resour. Res.* **2007**, *43*, W10414. [CrossRef]
32. Flammer, G.H.; Skogerboe, G.V.; Wei, C.Y.; Rasheed, H. Closed conduit to open channel stilling basin. *J. Irrig. Drain. Eng.* **1970**, *96*, 1–10. [CrossRef]
33. David, R.L.; Gregory, J.M. Evaluating the use of goodness of the fit measures in hydrologic and hydro climatic model validation. *Water Resour. Res.* **1999**, *35*, 233–241.